Published in final edited form as:
Neurotoxicology. 2013 January ; 34: 118–127. doi:10.1016/j.neuro.2012.10.018.

Manganese Transport via the Transferrin Mechanism

Thomas E. Gunter[a], **Brent Gerstner**[a], **Karlene K. Gunter**[a], **Jon Malecki**[a], **Robert Gelein**[b], **William M. Valentine**[c], **Michael Aschner**[d], and **David I. Yule**[e]

[a]Dept. of Biochem. and Biophys.; Univ. of Rochester School of Medicine and Dentistry, 601 Elmwood Ave.; Rochester, NY 14642, USA. brentgerstner@gmail.com, karlene_gunter@urmc.rochester.edu, jon_malecki@urmc.rochester.edu [b]Dept. of Environ. Med.; Univ. of Rochester School of Medicine and Dentistry; 601 Elmwood Ave.; Rochester, NY 14642, USA. bob_gelein@urmc.rochester.edu [c]Dept. of Pathology and Microbiology; Vanderbilt Univ. Medical Center; Nashville, TN 37232, USA. bill.valentine@Vanderbilt.edu [d]Dept. of Pediatrics and the Kennedy Center for Research on Human Development; Vanderbilt Univ. Medical Center; Nashville, TN 37232, USA. michael.aschner@Vanderbilt.edu [e]Dept. of Pharm. And Physiol.; Univ. of Rochester School of Medicine and Dentistry, 601 Elmwood Ave.; Rochester, NY 14642, USA. david_yule@urmc.rochester.edu

Abstract

Excessive manganese (Mn) uptake by brain cells, particularly in regions like the basal ganglia, can lead to toxicity. Mn^{2+} is transported into cells via a number of mechanisms, while Mn^{3+} is believed to be transported similarly to iron (Fe) via the transferrin (Tf) mechanism. Cellular Mn uptake is therefore determined by the activity of the mechanisms transporting Mn into each type of cell and by the amounts of Mn^{2+}, Mn^{3+} and their complexes to which these cells are exposed; this complicates understanding the contributions of each transporter to Mn toxicity. While uptake of Fe^{3+} via the Tf mechanism is well understood, uptake of Mn^{3+} via this mechanism has not been systematically studied. The stability of the Mn^{3+}Tf complex allowed us to form and purify this complex and label it with a fluorescent (Alexa green) tag. Using purified and labeled Mn^{3+}Tf and biophysical tools, we have developed a novel approach to study Mn^{3+}Tf transport independently of other Mn transport mechanisms. This approach was used to compare the uptake of Mn^{3+}Tf into neuronal cell lines with published descriptions of Fe^{3+} uptake via the Tf mechanism, and to obtain quantitative information on Mn uptake via the Tf mechanism. Results confirm that in these cell lines significant Mn^{3+} is transported by the Tf mechanism similarly to Fe^{3+}Tf transport; although Mn^{3+}Tf transport is markedly slower than other Mn transport mechanisms. This novel approach may prove useful for studying Mn toxicity in other systems and cell types.

Keywords

manganese transport; transferrin; endosomal transport; mitochondria; manganese toxicity

1. Introduction

While manganese (Mn) is an essential biological element and a necessary cofactor in a number of important enzymatic reactions, excessive brain Mn accumulation particularly in the globus pallidus and striatum can lead to neurotoxicity with symptoms and signs

Corresponding Author: Thomas E. Gunter, Dept. of Biochem. and Biophys.; Univ. of Rochester School of Medicine and Dentistry, 601 Elmwood Ave.; Rochester, NY 14642, USA thomas_gunter@urmc.rochester.edu phone: 1-585-275-3129 fax: 1-585-275-6007.

resembling those of Parkinson's disease. The evidence indicates that in the 2+ oxidation state (Mn^{2+}), Mn enters cells via a number of transport mechanisms, including the divalent metal transporter 1 (DMT1) (Au *et al*, 2008), a Mn citrate transporter (Crossgrove*et al*, 2003; Crossgrove and Yokel, 2004), a store activated Ca^{2+} channel (Yokel and Crossgrove, 2004), the ZIP8 mechanism (He *et al*, 2006; Liu *et al*, 2008), and the ZIP14 mechanism (Fujishiro *et al*, 2012; Girijashanker *et al*, 2008). In the 3+ oxidation state (Mn^{3+}) the evidence suggests that Mn is transported via the transferrin (Tf) mechanism (Aschner and Aschner, 1990; Aschner and Gannon, 1994). Mn uptake into a specific cell type is thus determined by the activity of each type of uptake mechanism expressed in that cell type and the oxidation state of the Mn reaching the cell. Once inside the cell, most of the Mn is found in the mitochondrial and nuclear fractions (Maynard and Cotzias, 1955).

A study of Mn speciation in animal cells using X-ray absorption near edge structure (XANES) spectroscopy identified only Mn^{2+} and a trace amount of Mn^{3+} having the spectrum of the enzyme Mn superoxide dismutase (Gunter *et al*, 2006a; Gunter *et al*, 2005; Gunter *et al*, 2004). This is undoubtedly because Mn^{2+} is by far the more stable species of these two oxidation states (Latimer and Hildebrand, 1956). The concentration of free Mn^{3+} is not zero, but exists in a steady state in which its concentration is much lower than that of free Mn^{2+} and below the XANES detection limit. A number of factors influence this steady state, but generally free Mn^{3+} is more stable at low pH than at neutral pH (Latimer and Hildebrand, 1956). Mn^{3+} can also enter aqueous solution when stabilized by formation of stable complexes (Gunter *et al*, 2006b), including some formed with common organic anions usually found in cells and tissue, such as citrate or Tf.

The Tf system is known to transport iron (Fe) primarily into mitochondria for incorporation into hemes and other Fe-containing proteins (Sheftel *et al*, 2007). Fe^{3+} transport via the Tf mechanism involves the following steps: binding of the Fe^{3+} to extracellular Tf, binding of the Fe^{3+}Tf complex to Tf receptors (TfRs) and movement of the Tf-bound TfR into clathrin-coated pits, invagination of these pits into endosomes bringing the Fe^{3+}Tf inside the cell, movement of the endosomes into the region of the cytosol in which the mitochondrial network is found, release of Fe^{3+} from binding to the Tf complex by acidification of the endosomal interior, reduction of the Fe^{3+} to Fe^{2+} by Steap proteins in the endosomes, transport of the Fe^{2+} out of the endosomes by DMT1, and uptake of the Fe^{2+} by mitochondria where it can be incorporated into hemes and other iron-containing proteins (Hentze *et al*, 2004; Ohgami *et al*, 2005; Ohgami *et al*, 2006; Richardson and Ponka, 1997; Sheftel *et al*., 2007).

Mn and Fe are elements with atomic numbers 25 and 26, respectively, within the transition metal series and have many similar characteristics. Mn uptake via the Tf mechanism has usually been assumed to be analogous to that of Fe; nevertheless, there are differences in their chemistry, which could cause Mn^{3+} transport via Tf to differ from transport of Fe^{3+}. First, the oxidation state in which Fe binds most strongly to Tf, Fe^{3+}, is also its most stable oxidation state at physiological pH; in contrast, while Mn also binds Tf as Mn^{3+}, it is most stable at physiological pH as Mn^{2+}. Since the concentration of free blood Mn^{3+} is very low at physiological pH, even when Mn is present in excess, mass action would predict that Mn^{3+} would bind to Tf very slowly as Mn^{3+} transferrin (Mn^{3+}Tf). This is supported by the observation that the procedure set up by Aisen et al. for preparing Mn^{3+}Tf requires a week for the accumulation of the stable Mn^{3+}Tf complex to approach completion (Aisen *et al*, 1969). We have studied this slow conversion of Mn^{2+} to Mn^{3+} more closely under somewhat more physiological conditions in a XANES experiment described below. Studies of transport of Fe^{3+} via the Tf mechanism show that the Fe^{3+} is reduced to Fe^{2+} by Steap proteins inside endosomes and transported out of the endosomes via DMT1 (Hentze *et al*., 2004; Ohgami *et al*., 2005; Ohgami *et al*., 2006; Richardson and Ponka, 1997). Mn^{2+}, like

Fe^{2+} is transported by DMT1 (Au *et al.*, 2008) and hence should be released from the endosomes similarly to Fe^{2+}. Furthermore, the Tf transport mechanism for Fe is known to deliver Fe^{2+} to the vicinity of the mitochondrial network, where it is sequestered into mitochondria for incorporation into hemes (Sheftel *et al.*, 2007). If it also delivers Mn^{2+} to mitochondria, it could contribute to mitochondrial Mn toxicity associated with deficits in energy production (Brouillet *et al*, 1993; Galvani *et al*, 1995; Gavin *et al*, 1992; Malecki, 2001; Malthankar *et al*, 2004; Roth *et al*, 2000; Roth *et al*, 2002; Zwingmann *et al*, 2003)

The systems transporting Mn^{2+} into cells are complex and difficult to functionally isolate experimentally. Furthermore, the expression of each type of transporter varies with cell type. However, we have been able to purify the Mn^{3+}Tf complex and also to covalently bind a fluorescent label (Alexa green) to Mn^{3+}Tf because of the stability of this complex. This has permitted us to study the transport of Mn via the Tf mechanism independently of the other cellular Mn transport mechanisms, to follow the transport of Mn^{3+}Tf into neuronal cells and into the region of the mitochondrial network using confocal microscopy, and to confirm that Mn transport via the Tf system functions analogously to the transport of ferric iron (Fe^{3+}) by this mechanism. Using the purified Mn^{3+}Tf and atomic absorption spectroscopy (AA), we have also been able to measure the accumulation of Mn via Mn^{3+}Tf independently of the other Mn transport mechanisms using atomic absorption and to compare it with the accumulation from a similar concentration of Mn^{2+}. The primary goal of the work reported here is to introduce this novel approach to the study of transport of Mn^{3+} via the Tf system to those interested in its role in Mn neurotoxicity so that it may be applied to studies of Mn^{3+}Tf transport in additional systems and cell types and to more complete studies of its uptake kinetics.

The uptake of Mn^{3+} via the Tf mechanism in the two neuronal cell types used in the current study is slower than that of Mn^{2+}, but isn't negligible and therefore could contribute to Mn toxicity, along with Mn transported into cells by the other transport mechanisms. However, this does not necessarily mean that transport of Mn^{3+} via the Tf system is so small in all cell types and so other cell types should be studied. Furthermore, Mn^{3+} is also a strong oxidizing agent, which might be expected to oxidize many components of the endosome in addition to the Steap proteins. Thus, transport of Mn via the Tf mechanism exposes an additional set of cell components to Mn, particularly within the endosomal system, which could be damaged by this transport process, but not by other processes of Mn transport into the cell.

2. Materials and Methods

2.1 Neuronal Cells

Mn uptake via the Tf mechanism was studied in cultured mouse hippocampal (HT22) and striatal neurons (STHdhQ7/Q7) (Trettel *et al*, 2000). The latter were chosen because the striatum is an area where Mn preferentially accumulates, and one of the areas most affected by Mn toxicity (Finkelstein *et al*, 2007). HT22 cells were grown at 37° C in an incubator with 5% CO_2 in Gibco F-12 mixture (HAM) containing 5% FBS, 5% HS, 20 mM glucose, and Pen Strep. The STHdhQ7/Q7 cells were grown at 33° C with 5% CO_2 in Gibco F-12 containing 10%FBS, 5% HS and Pen Strep. Both cell types were passed with 0.05% trypsin and 0.53 mM EDTA about every 3 days. For long term storage, each type of cell was frozen in 90% fetal calf serum/10% DMSO and stored in a liquid nitrogen refrigerator at 77° K. The cells were used between passages 3 and 7.

2.2 XANES Spectroscopy

XANES spectroscopy is a technique similar to extended X-ray absorption fine structure (EXAFS) in which an energy shift is observed between the absorption edges of different

oxidation states of an element. Furthermore, unlike some spectroscopies, such as electron paramagnetic resonance (EPR), where some spectra may be relaxation broadened to the point where they are no longer observable, XANES spectroscopy shows the spectra of all compounds and complexes containing the element of interest weighted by their abundance, with spectra of each oxidation state found near its appropriate absorption edge. These absorption edges are separated by several electron volts, a difference which is easily measurable. This makes XANES spectroscopy the "gold standard" for determining the oxidation state or states of an unknown biological compound or complex containing the element of interest. The details of the techniques used and methods of handling the XANES sample described here are outlined in the Supplemental Material and more completely in earlier publications (Gunter *et al.*, 2006a; Gunter *et al.*, 2005; Gunter *et al.*, 2006b; Gunter *et al.*, 2004).

A sample of Mn^{2+} (0.2 mM) with Tf (2 mM) in HEPES (10 mM) buffered saline (160 mM Na^+ and Cl^- pH 7.2) was allowed to incubate at room temperature (22° C) for 24 hours. Polymerized dextran (10% w/v final concentration) was mixed into the sample, which was rapidly frozen using liquid nitrogen and maintained at −80° C until XANES spectroscopy could be carried out at beamline 9 B at the National Synchrotron Light Source at Brookhaven National Laboratory. The polymerized dextran aids in producing a glassy sample and minimizing the formation of ice crystals, which could distort the spectrum by inducing Bragg reflections. The sample's XANES spectrum was analyzed by curve fitting to a set of Mn^{2+} and Mn^{3+} standards (model compounds) as previously described and as illustrated in Figs. S1 and S2A and S2B in the Supplementary Material (Gunter *et al.*, 2006a; Gunter *et al.*, 2005; Gunter *et al.*, 2006b; Gunter *et al.*, 2004).

2.3 Construction and Characterization of Probes

2.3.1 Mn^{3+} Transferrin—Apotransferrin (Apo-Tf) purchased from Lee BioSolutions, St Louis, MO was shown by sodium dodecyl sulfate polyacrylamide gel electrophoresis (SDS-PAGE) to fractionate as a single band at approximately 77 kD. Mn^{3+} was bound to Tf using a modification of the technique of Aisen et al (Aisen et *al.*, 1969). Briefly, a three fold excess of a 1:1 solution of Mn^{2+} and citrate (pH 5.0) was mixed with a 5% solution of apotransferrin in 0.1 M KCl and incubated in a cold room (4°C) for about a week. During the incubation, the very light pink color of Mn^{2+} slowly assumes the dark grayish color of Mn^{3+}. At the end of this incubation the suspension was carefully inspected visually for the presence of any precipitate. There was no evidence of a precipitate. The suspension was then spun in Vivaspin 15 tubes made by Sartorius Stedim to separate the Mn^{3+}-bound Tf from the medium. These tubes contain a 30 kD MWCO filter which passes the small ions and molecules and retains the Tf (~ 77 kD). The retentate was collected from the filter, diluted in medium (0.1 M KCl, 0.05 M K Tris, pH 7.5), and recentrifuged up to 35 times in order to separate and remove the free Mn^{2+} and any other small impurities from the Tf solution. In this medium the only component which could bind the Mn was the Tf. The final solution from this purification was tested by visible/UV spectroscopy to verify that its spectrum was similar to the published Mn^{3+}Tf spectrum (Aisen et *al.*, 1969). It was also tested by EPR to determine the amount of Mn^{2+} hexahydrate (free Mn^{2+}) remaining, by atomic absorption (AA) to determine the total Mn present, and by the Bradford assay to determine the amount of protein (i.e. Tf) present. The amount of Mn^{2+} found using the EPR assay represented less than 1% of the total Mn found by AA in all probes and at around 0.2 % in the probe used for quantitative Mn uptake measurements by AA in the work reported here. The results of these measurements allowed determination of the number of Mn^{3+} ions bound per Tf molecule. For the quantitative probes used in the current work, the Mn^{3+}/Tf ratio was in the range 1.6 to 2.0. The purified probes were stored at −20°C until they were used in experiments.

2.3.2 Attachment of Alexa green 488 to transferrin—Alexa Fluor 488 carboxylic acid succinimidyl ester (amine binding reagent) was purchased from Invitrogen (A-20000) and attached to the Apo-Tf using the manufacturer's suggested protocol. Briefly, 16 mg of Tf was dissolved in 1 ml of 0.1 M $NaHCO_3$ buffer (pH 8.3). The Alexa green (AG) 488 amine reactive compound was dissolved in 0.5 ml of DMSO at a concentration of 10 mg/ml. The amine reactive solution was slowly added to the Tf solution as it was being stirred, and the resulting solution was incubated for 1 hr at 22°C. The Tf plus AG-reactive probe was dialyzed in a cold room overnight with several changes of buffer. The AG-Tf was then carried through the procedure described under section 2.3.1 "Mn^{3+} Transferrin" to bind Mn^{3+} to the labeled Tf (forming $AGMn^{3+}Tf$). During the week of incubation, the beaker containing the AG-Tf was wrapped in aluminum foil and generally kept in the dark to minimize bleaching. Following the Vivaspin 15 purification centrifugations, final product was not diluted, but the concentration of Tf was measured using the Coomassie-stained SDS-PAGE technique described below. Binding of the fluorescent AG moiety to the Tf molecule is unlikely to affect the binding of Mn^{3+} to Tf significantly since the AG binding procedure used targets amine groups, particularly the terminal amine, and not the Mn^{3+} binding sites. The stability of the AG labeled probe was checked in the same way as that of the unlabeled probe, as described in the Supplementary Material, and the probe was found to be stable.

2.4 Protein Measurements

Protein measurements were carried out with the Bradford technique except in those cases where Alexa green 488 had been bound to Tf. The Bradford assay could not be used with $AGMn^{3+}Tf$, because the intense absorbance of the fluorescent label dominated the spectrum necessary for protein measurements. For measurements of the amount of protein in $AGMn^{3+}Tf$ solutions, the protein was run on an SDS-PAGE gel, labeled with Coomassie blue and the total color of the band integrated and compared with that of several known concentrations of $Mn^{3+}Tf$.

2.5 EPR analysis of probes

EPR was used to compare the amount of Mn^{2+} hexahydrate (free Mn^{2+}) present at the beginning of the $Mn^{3+}Tf$ incubation, the amount present at the end of the incubation (after approximately 1 week at 4° C), and the amount present at the end of the "clean up spins". At that time, the amount of Mn^{2+} hexahydrate present was compared with the total Mn present measured using atomic absorption spectroscopy (see "Mn Transferrin"). The measurements were carried out using an X-band Bruker EPR spectrometer modified as described (Black and Swarts, 2010) and utilizing an IBM Instruments Inc. microwave bridge system (ERO42MRH). During these measurements, samples were in quartz EPR flat cells in one part of a Varian dual cavity system; the other part of the dual cavity held a $CuCl_2$ standard. The six line derivative spectrum of Mn^{2+} hexahydrate in the sample was compared with that of a Mn^{2+} hexahydrate standard of known concentration at 22 °C. While the spectra of the pre- and post- incubation samples could be easily seen because of the excess Mn^{2+} concentration used with respect to the concentration of transferrin, the EPR spectra of the samples carried through the Vivaspin 15 centrifugations required extensive computing of average transients in order to bring the noise down to a level where the spectrum could be interpreted. During all of these measurements, the klystron power and modulation amplitudes were kept the same for all samples varying only the signal gain. The EPR spectrum of the $Mn^{3+}Tf$ itself cannot be seen in these spectra because of extreme relaxation broadening commonly seen with low symmetry Mn^{3+} compounds at room temperature (Abragam and Bleaney, 1970; Vincent and Love, 2012). Additional information and typical EPR spectra are shown in Fig. S3B of the Supplemental Material.

2.6 UV-visible analysis of probes

UV-visible spectra were taken of the probes used in order to visualize the appearance of the UV-visible spectrum of Mn^{3+}Tf both before the incubation and at the end of the "clean up" spins. These measurements were carried out on a Varian Cary 100Bio UV-Visible spectrometer. The spectrum of Mn^{3+}Tf which had not been bound to Alexa green 488 looked identical to that published in Fig. 1 of Aisen et al (Aisen et *al.*, 1969), while the spectrum of AGMn^{3+}Tf also showed the strong absorbance of the Alexa green with a peak at 488 nm. Additional information on the UV/visible spectra of Mn^{3+}Tf in these probes showing the known UV/visible spectrum of Mn^{3+}Tf is shown in Fig. S3B of the Supplemental Material.

2.7 Atomic absorption analysis of the probes and of Mn uptake

Total Mn present in the probes and in cell samples was measured using a Perkin-Elmer AAnalyst 600 atomic absorption spectrometer equipped with a THGA (transversely-heated graphite furnace) and Mn Lumina™ hollow-cathode lamp (Perkin-Elmer Part No. N305-0145)(279.5 nm, slit 0.2 nm). To calibrate the spectrometer for Mn, reference solutions (containing 0, 2, 5, 10, and 20 μg/l Mn) were prepared daily in 2% HNO_3 from a commercial spectroscopically pure 1000 mg/L Mn stock solution (SPC Science Cat. No. 140-051-250). Nine measurements were made for each sample. For each measurement, 20 μl of sample (or standard) was mixed with 5 μl of a 0.05% (w/v) Pd + 0.03% (w/v)$Mg(NO_3)_2$ matrix modifier and injected into the furnace with an automated sampler (Perkin-Elmer AS800). The temperature program used pyrolysis at 1300°C and atomization at 2000º C. Ultra-pure nitric acid (Seastar Chemicals Inc.; Sidney, BC, Canada) was used throughout sample preparation and standards and the matrix modifier was prepared from 10 g/L Pd and 10 g/L $Mg(NO_3)_2$ (Perkin-Elmer Part Nos. BO19-0635 and Bo 19-0634, respectively). Ultrapure water, resistivity 18 MΩ cm^{-1} obtained from a Barnstead/Thermolyne Diamond Life Science (Dubuque, IA)(UV/UF) ultrapure water system was used for all solutions.

2.8 Confocal Microscopy

AGMn^{3+}Tf was used to follow the binding of Tf to the TfR on the plasma membrane of the neuronal cells and the passage of the Tf through the endosomes into the region of the mitochondrial network. Mitotracker red and Mitotracker green were used in different experiments to identify mitochondria within each neuronal cell. If Mitotracker red or green were to be used in the experiment, they were added to the medium above the cells and incubated for 20 min prior to mounting the cover slip on the stage of the confocal microscope. The neuronal cells had settled on and attached to a 15 mm cover slip, which was placed in a Warner Instruments RC-25F chamber. The imaging buffer used contained 137 mM NaCl, 0.56 mM $MgCl_2$, 4.7 mM KCl, 1 mM Na_2HPO_4, 10 mM HEPES (pH 7.4), 5.5 mM glucose and 1.26 mM $CaCl_2$. The RC-25F chamber containing the cover slip was mounted in a Warner Instruments Platform-Series 20 PH1 system on the microscope stage, which allowed fresh medium to flow into the RC-25F chamber over the cover slip. At a time designated as time zero the desired amount of AGMn^{3+}Tf was added to the RC-25F chamber and allowed to incubate for 1 min. The unbound AGMn^{3+}Tf was then washed away with fresh medium. The progress of the AGMn^{3+}Tf in binding to the TfR, being incorporated into endosomes, and passing into the region of the cytosol near the mitochondrial network was then followed by periodically taking images of the cells. White light images and in some cases Z stacks were also taken to better show the cell boundaries (membranes) and the distribution of the probes within the cells.

Images were acquired simultaneously for each dye using a Nikon C1-LU3 visible light laser scanning confocal microscope with a 60× (1.4 NA) oil immersion objective. The suite of

lasers and capture of images was controlled through EZ-C1 software. Alexa green 488 and mitotracker green were excited by the 488 nm argon laser line and emission was collected through a 543 nm bandpass filter and photomultiplier. Mitotracker red CMXRos was excited by the 543 nm line from a He-Ne laser, and emission was collected through a 585 ± 30 nm bandpass filter and photomultiplier.

2.9 Uptake of Mn^{3+}Tf by Neuronal Cells

The protocol developed for washing the cells and preparing them for measurement of uptake by atomic absorption was very similar to that used to pass the cells and was designed to be both thorough and gentle. Cells of both types were grown to 70 – 80% of confluence in 6 well dishes containing 2.25 ml of medium per well (Gibco F-12 mixture (HAM) containing 5% FBS, 5% HS, 20 mM glucose, and Pen Strep) and throughout the following procedure kept at either 37° C for the HT22 cells or 33° C for the STHdhQ7/Q7 cells. During a change of medium (2.5 ml of fresh medium), 1.11 μM cyclosporin A was also added as insurance against induction of the mitochondrial permeability transition. After 15 minutes, in three separate experiments, either 100 μM purified Mn^{3+}Tf (final concentration), 100 μM Mn^{2+} (chloride) (final concentration), or the amount of Mn^{2+} (chloride) measured by EPR at the end of the purification (0.2 μM), diluted by the same factor that the Mn^{3+}Tf stock had been diluted to reach 100 μM (another factor of ten or 0.02 μM), was added to each well. At the appropriate time, the medium containing either Mn^{3+}Tf or Mn^{2+} was removed with a pipette and the cells carefully washed twice with 2 ml of phosphate buffered saline (PBS) (137 mM NaCl, 2.7 mM KCl, 4.3 mM Na_2HPO_4, and 1.4 mM KH_2PO_4, pH 7.2). The cells were then removed from the dishes as follows: 0.25 mg/ml pronase in 1 ml of medium was added to the dish which was swirled gently and allowed to stand for 20 min. This medium was then removed and the dish was washed twice with PBS medium. At each step in this protocol the cells were inspected for damage by light microscopy. Cell medium containing 0.05% trypsin and 0.53 mM EDTA (as described above under “Neuronal Cells”) was added, and the cells were removed from the bottom of the well by the stream of medium from a transfer pipette. Next, the the trypsin-containing medium was transferred to an Eppendorf tube, and the cells were centrifuged in a Hermle centrifuge for 1 min at 10,000 rpm. The supernatant was then poured off and the pellet carefully rinsed 3 times with 1 ml of PBS. The cells were then resuspended in 1 ml of PBS. The centrifugation and rinsing steps were repeated once or twice. The resulting pellet was resuspended. Aliquots of some pellets were replated and inspected with a light microscope to ensure that the cells were intact and appeared healthy. The resuspended cells were lysed by suspension in 1 ml of double distilled water and maintained at 4° C until the end of the uptake experiment when all of the samples from the experiment were frozen. When all the samples were complete, they were thawed, carefully vortexed to insure proper mixing, and measured with AA and the Bradford assay, as described above.

2.10 Statistics

Means and standard deviations of the data and fitting lines to the data were determined using Excel© software. While it appears obvious that the points representing uptake from 100 μM Mn^{3+}Tf and from 0.2 μM Mn^{2+} in Fig. 4 A and B and those representing uptake from 100 μM Mn^{3+}Tf and 100 μM Mn^{2+} in Fig. 5 A and B are significantly different, this was quantified by the usual procedure of assuming the null hypothesis of a common population and showing that this hypothesis is rejected at above the 99% level. This was done by comparing the 24, 36, and 48 hour points in Fig. 4 and the 6 and 12 hour points in Fig. 5 using Willcoxon Mann-Whitney tests as described in “Statistical Methods” (Snedecor and Cochran, 1989). We used the Vassar Statistical Computation Web Site established by Prof. Richard Lowy (faculty.vassar.edu/lowy/utest.html).

3. Results

3.1 Conversion of Mn^{2+} to Mn^{3+} through stabilization in a Tf complex

An experimental sample containing separately added Mn^{2+} (0.2 mM) and Tf (2.0 mM) was incubated at 22° C for 24 hr in HEPES (10 mM) (pH 7.2) buffered saline (160 mM NaCl). The sample was then frozen and maintained at −80° C until a XANES spectrum could be obtained (Fig. 1). The sample was analyzed with curve-fitting techniques in which its spectrum was compared with the spectra of the Mn^{2+} and Mn^{3+} model compounds shown in Fig. S2 A & S2 B in the Supplementary Material. These techniques are described in detail in four earlier papers (Gunter et *al.*, 2006a; Gunter et *al.*, 2005; Gunter et *al.*, 2006b; Gunter et *al.*, 2004). The results showed that after the 24 hr incubation, the sample had acquired approximately 18% Mn^{3+}. This shows that Mn^{3+}Tf does form, albeit slowly, from Mn^{2+} at neutral pH. It also shows that the Mn^{3+}Tf complex is capable of holding Mn^{3+}Tf stably over time.

3,2 Binding of Alexa green labeled Mn^{3+}Tf to cell membranes, formation of endosomes and transport of the Alexa green labeled Mn^{3+}Tf via the endosomes into the region of the mitochondrial network

As can be seen in Figs. 2A and 2B, AGMn^{3+}Tf binds rapidly within a 1 min incubation period to the membranes of both HT22 neurons (Fig. 2A) and STHdhQ7/Q7 neurons (Fig. 2B). The green color shows the location of the Mn^{3+}Tf, and the red color (Mitotracker red) shows the location of the mitochondrial network in these cells. These sets of images were taken 2 min (to account for the time required to wash away unbound AGMn^{3+}Tf) and 16 min after addition of AGMn^{3+}Tf. The 16 min images show that the green labeled vesicles have moved farther into the cell than they had at 2 min. Over the initial 16 min of these experiments, the movement of the AGMn^{3+}Tf can be followed as the green fluorescence emission moves from the membrane towards the region of the mitochondrial network. Similar experiments, carried out without mitotracker dyes showed no essential difference in the behavior and movement of the green color (AG label). The mitotracker dyes were only used to indicate the area of the mitochondrial network and no attempt was made to determine whether mitochondria take up the Mn *per se*. As with Fe^{3+}Tf, Mn^{3+}Tf uptake likely takes place within endosomes (Hentze et *al.*, 2004; Richardson and Ponka, 1997), although these organelles do not appear in the images Fig. 3A & B because they are smaller than the resolution of the optical system. The Z-plane of the images shown in Fig. 2A and 2B was about 0.5 μm above the cover slip. Apparent inclusion of a few green spots and even mitochondria in the nuclei in some of the cells indicates that a few green endosomes and mitochondria are trapped between the nuclear membrane and plasma membrane in these images.

The AG probe which had not reacted with the Tf molecule during synthesis of AGMn^{3+}Tf was dialyzed away from the AGMn^{3+}Tf using fresh medium (see “Attachment of AG488 to transferrin”), made non reactive, saved separately from the AGMn^{3+}Tf and subsequently used as a control in experiments similar to those described in Fig. 2A and 2B above. This unattached AG could easily be seen before being washed away after 1 min of incubation with the cells; however, almost all of it was washed away when the cells were washed. There was no indication of extensive binding to the exterior of the cells and the formation of AG labeled endosomes as there was with the AGMn^{3+}Tf treated samples.

Figs 3A and 3B show a time sequence of AGMn^{3+}Tf uptake in typical samples of HT22 neurons (Fig. 3A) and STHdhQ7/Q7 neurons (Fig. 3B). Uptake was quantified by drawing regions of interest just inside the plasma membrane of these cells as shown in the Supplementary Material (Fig. S4) and using “Image J” software (available from the NIH) to

show the relative amount of green emission from inside the cell as a function of time. The average intensity of this green fluorescence is shown quantitatively in Fig. 3A for HT22 neurons and in Fig. 3B for STHdhQ7/Q7 neurons. Because it takes at least 1 min to wash off the external AGMn^{3+}Tf from the cover slip in the field of the confocal microscope, the first uptake data that can be analyzed in this way is 2 to 3 min after addition of the AGMn^{3+}Tf to the medium above the neurons. By this time, the amount of AGMn^{3+}Tf found inside the cells is already significant. It continues to increase for approximately 5 to 6 more min before complete saturation. Even though the intensity of the average green fluorescence inside the cells saturated at about 5 or 6 min after addition of the AGMn^{3+}Tf probe, movement of the green fluorescence away from the cell membranes continued for another 10 or 11 min. Therefore, 16 min was chosen in the second row of panels in Fig. 2A and 2B to provide some information on this additional movement of the AGMn^{3+}Tf.

3.3 Competition between Fe^{3+}Tf and Mn^{3+}Tf for transport via the Tf mechanism and inhibition of this transport by chlorpromazine and dynasore

Figs. 3A (HT22 hippocampal neurons) and 3B (STHdhQ7/Q7 striatal neurons) show strong competitive inhibition of AGMn^{3+}Tf transport by Fe^{3+}Tf added to the RC25F chamber prior to addition of the same amount of AGMn^{3+}Tf used in acquiring the images shown in Fig. 2A and 2B and the quantitative data in Figs. 3A and 3B. However, the inhibition seems stronger for the STHdhQ7/Q7 striatal neurons. Chlorpromazine and dynasore are classical inhibitors of Fe^{3+}Tf binding to the TfR and its subsequent incorporation into clathrin-coated pits and endosomes (Ivanov, 2008). Addition of these inhibitors (both from Sigma Chem. Co.; St. Louis, MO) to the RC25F chamber prior to addition of AGMn^{3+}Tf greatly reduces uptake of AGMn^{3+}Tf in both HT22 (Fig. 3A) and STHdhQ7/Q7 neurons (Fig. 3B), with stronger inhibition in the STHdhQ7/Q7 neurons. This finding provides further evidence that Mn^{3+} uptake occurs similarly to that of Fe^{3+} by the Tf mechanism.

3.4 A comparison of uptake of purified Mn^{3+}Tf with uptake of Mn^{2+}

3.4.1. Uptake of residual Mn2+ present as an impurity—Fig. 4A compares the uptake of purified Mn^{3+}Tf into HT22 hippocampal neurons from a 100 μM solution of purified Mn^{3+}Tf with that of Mn^{2+} from a 0.02 μM solution of Mn^{2+} using the AA technique described in the Methods section. 0.2 μM was the concentration of free Mn^{2+} measured as an impurity by EPR in the purified Mn^{3+}Tf stock samples. This 0.2 μM was then diluted by an additional factor of ten to match the dilution of the Mn^{3+}Tf stock in setting up the 100 μM Mn^{3+}Tf samples. Fig. 4B shows results of the same experiment using STHdhQ7/Q7 striatal neurons. In both cases, uptake from the 100 μM Mn^{3+}Tf solution was much greater than that from 0.02 μM Mn^{2+}. Willcoxon Mann-Whitney tests in each case indicate significance at the 99.9% level. Thus the uptake from the 0.02 μM Mn^{2+} impurity cannot account for the uptake observed from the purified Mn^{3+}Tf solutions. Therefore, the uptake from Mn^{3+}Tf is real and significant. The actual uptake of Mn from the 100 μM Mn^{3+}Tf samples should be thought of as the difference between these two curves.

3.4.2. Uptake rates of equal amounts of Mn^{3+}Tf and Mn^{2+}—Figs. 5A and 5B compare initial rates of uptake of Mn from 100 μM purified Mn^{3+}Tf with that from the same molar concentration (100 μM) of Mn^{2+} in hippocampal and striatal neurons, respectively. The uptake of Mn^{2+} was markedly faster in both cases than that of transport via the Tf mechanism. That these data represent separate populations with uptake from 100 μM Mn^{2+} significantly greater than that from 100 μM Mn^{3+}Tf was established using Willcoxon Mann-Whitney tests at the 99.4% level.

4. Discussion

While Fe uptake via the Tf mechanism has been thoroughly studied and described in a large number of publications over the last 30 years, the transport of Mn via this mechanism has not been systematically studied. Initial evidence that Mn could be transported into cells via the Tf mechanism was published over 20 years ago (Aschner and Aschner, 1990); however, many of the characteristics of this transport have remained speculative and significant differences may exist between Fe and Mn transport via this mechanism. For example, Mn^{2+} is the most stable state of free Mn at the pH found in extracellular fluid while Fe^{3+} is the most stable state of Fe under the same conditions (Latimer and Hildebrand, 1956). In addition, since Mn^{3+} (Standard Reduction Potential E = 1.51) is a much stronger oxidizing agent than Fe^{3+} (E= 0.77), there could be significant differences in the transport behavior of these two transition metals via this Tf mechanism (West, 1971). Steap proteins II through IV have evolved to reduce Fe^{3+} to Fe^{2+} within the endosomes so that the Fe^{2+} can be transported out of the endosomes via the DMT1 mechanism (Ohgami et *al.*, 2005; Ohgami et *al.*, 2006; Sheftel et *al.*, 2007); however, Mn^{3+}, is a strong enough oxidizing agent that it could oxidize endosomal components other than the Steap proteins, and in the process it could damage the endosomes and the cell. This type of damage would not be directly visible using confocal microscopy because of the small size of the endosomes, but it could constitute an additional mechanism of Mn toxicity. Mn transport via the Tf mechanism could also induce toxicity through the same mechanisms as transport of Mn^{2+} into the cell.

The XANES data shown in Fig. 1 clearly establish that Mn^{3+}Tf can be slowly formed from Mn^{2+} and Tf at neutral pH in saline, thus strongly suggesting that this will also occur in extracellular fluid. The speed of formation of Mn^{3+}Tf in extracellular fluid will undoubtedly vary with Mn and Tf concentrations, pH, and the concentration of other stabilizing compounds such as citrate.

The small green sources of emission seen moving into the cytosol in the AGMn^{3+}Tf data shown in Fig. 2A and 2B appear similar to what would be expected if Mn^{3+} transport via the Tf mechanism involves endosomes and is a close analog of what Fe^{3+} transport via this mechanism is believed to be (Hentze et *al.*, 2004; Ohgami et *al.*, 2005; Ohgami et *al.*, 2006; Richardson and Ponka, 1997; Sheftel et *al.*, 2007).

The uptake rate of AGMn^{3+}Tf shown in Fig. 3 A and B appears to be more rapid than the accumulation of Mn in the cells shown in Fig. 4 and 5; however, these experiments employed two different types of measurements and measured different things. Of the two types of measurement, fluorescence is much more sensitive than AA. The fluorescence data in Fig. 3 show the AG accumulation in the cell interior, which saturates when the cycling of the TfR between the endosomes and the plasma membrane reaches steady state. The AA data in Fig. 4 and 5 show the accumulation of Mn itself in the cells. It takes numerous cycles of transport via the Tf mechanism (as seen in the fluorescence experiments) to build up the amounts of Mn seen inside the cells by AA. Even this relatively slow Mn accumulation via the Tf mechanism inside the cells (Fig. 4 and 5) is undoubtedly faster than the Mn accumulation which would occur via the Tf mechanism i*n vivo*, because the concentration of free Mn^{3+} prior to its binding to Tf *in vivo* is very low. Furthermore, because the iron concentration of the extracellular fluid is high, much of the Tf would be expected to be bound by Fe^{3+}. Nevertheless, because the Mn^{3+} concentration is not zero, mass action would allow very small amounts of Mn^{3+} to bind to Tf and to be transported via the Tf mechanism (Vincent and Love, 2012). In the experiments shown in Fig. 4 and 5, we have avoided these concentration-induced bottlenecks by binding Mn^{3+} to Tf and purifying the complex prior to the experiments.

The data shown above (Fig. 3A and 3B) also show that Fe^{3+} competes with Mn^{3+} for uptake via the Tf mechanism and that this Mn^{3+}Tf transport is inhibited by classical inhibitors of the clathrin-coated pit mechanism, chlorpromazine and dynasore, confirming that Mn transport is similar to Fe transport via the Tf mechanism (Ivanov, 2008).

In addition, the experiments comparing the rate of uptake of purified Mn^{3+}Tf with that of Mn^{2+} at equal concentrations (Fig. 5 A & B) show that Mn^{3+}Tf is transported via this classically described, Fe-specific mechanism, although it is taken up more slowly than a similar concentration of Mn^{2+} by one or more of the Mn^{2+}-transporting mechanisms in both types of neurons. 100 μM Mn^{2+} is sequestered about 8.5 fold faster than the Mn^{3+}Tf in HT22 hippocampal neurons and about 8.6 fold faster in STHdqQ7Q7 striatal neurons in these data. This is true even though the protocol used Mn^{3+} which had already been stabilized by binding to Tf, eliminating the step in which Mn^{3+} associates with the Tf, which must be a bottleneck to the process *in vivo*. Therefore, the uptake velocities measured here should not be taken as what would be seen *in vivo*, but should be taken to represent uptake into these two types of neurons via the Tf mechanism when the probable rate-limiting step is bypassed. Since the concentration of Mn^{2+} used in the uptake studies (100 μM) was in the upper end of the physiological range or lower end of the pathological range found in cells and tissue (Gunter et *al.*, 2005; Gunter et *al.*, 2004), it might be argued that there could be saturation effects influencing the uptake rate in the Mn^{2+} data. Even if this is true, the uptake of Mn^{2+} is so much faster than that of the Mn^{3+}Tf at the same concentration that these two sets of data can be shown to represent two statistically distinct populations reinforcing the conclusion that uptake of Mn^{2+} into these cells is significantly greater than that of Mn^{3+}Tf. These results and arguments suggest that Mn^{3+} uptake via the Tf mechanism into these types of neurons is small and much smaller than that of Mn^{2+} via other mechanisms.

The results of the experiments described here suggest that: 1) A significant amount of Mn^{3+} can be transported into neuronal cells via the Tf mechanism. 2) This transport shows characteristics similar to those of Fe^{3+} transport via this same mechanism. 3) The amount of this transport in the two lines of neuronal cells used was small and much less than transport of Mn^{2+} via other transport mechanisms. 4) In addition to contributing to the same mechanisms of toxicity as other mechanisms of Mn uptake into cells, because Mn^{3+} is a strong oxidizing agent, Mn^{3+} transport via the Tf mechanism, could also cause oxidative damage at the endosomal level. More complete answers to issues raised here such as transport kinetics, endosomal damage, and amounts of Mn^{3+}Tf transport in other cell types (e.g. astrocytes) will require further study.

Supplementary Material

Refer to Web version on PubMed Central for supplementary material.

Acknowledgments

The authors would like to thank Dr. William Bernhard for use of his EPR and UV-visible spectrometers and Mr. Paul Black for instructions on the use and help in operating these spectrometers. They would like to thank Dr. Marcy MacDonald for developing and permitting us to use the STHdhQ7/Q7 striatal neurons and Dr. Gail Johnson-Voll for providing us with these cells. They would like to thank Dr. Pamela Meher for providing us with the HT22 hippocampal neurons. They thank Dr. Beth Van Winkle for help with cells. They thank Dr. Lisa Miller and Dr. Nebojsa Marinkovic and other personnel of beamline 9B of the National Synchrotron Light Source (NSLS) at Brookhaven National Laboratory for use of their facilities and assistance with the XANES experiments. They thank Dr. Harold Smith for important discussions on techniques used in this work and Dr. Andrei Ivanov for helpful discussions about the clathrin-coated pit mechanism of formation of endosomes. They thank Dr. Claire Gavin for editing and suggestions for clarity in the wording of the manuscript and both Dr. William Simon and Ms. Kelly Gunter for consultations on statistics. Research described in this article was supported by NIH RO1 ES10041. The NSLS is supported by the United States Department of Energy under contract DE-AC02-98CH10886.

Abbreviations

Tf	transferrin
Mn^{3+}Tf	Mn^{3+} bound to transferrin
DMT1	divalent metal transporter 1
XANES	X-ray absorption near edge structure spectroscopy
TfRs	transferrin receptors
EXAFS	extended X-ray absorption fine structure
EPR	electron paramagnetic resonance
Apo-Tf	Apotransferrin
AA	atomic absorption
AG	Alexa green
AGMn^{3+}Tf	Alexa green manganese transferrin

References

Abragam, A.; Bleaney, B. Electron Paramagnetic Resonance of Transition Ions. Clarendon Press; Oxford: 1970.

Aisen P, Aasa R, Redfield AG. The chromium, manganese, and cobalt complexes of transferrin. J Biol Chem. 1969; 244:4628–4633. [PubMed: 4309148]

Aschner M, Aschner JL. Manganese transport across the blood brain barrier: Relationship to iron homeostasis. Brain Res Bull. 1990; 24:857–860. [PubMed: 2372703]

Aschner M, Gannon M. Manganese (Mn) transport across the rat blood-brain barrier: Saturable and transferrin-independent mechanisms. Brain Res Bull. 1994; 33:345–349. [PubMed: 8293318]

Au C, Benedetto A, Aschner M. Manganese transport in eukaryotes: the role of DMT1. Neurotoxicology. 2008; 29:569–576. [PubMed: 18565586]

Black PJ, Swarts SG. Ex vivo analysis of irradiated fingernails: chemical yields and properties of radiation-induced and mechanically-induced radicals. Health Physics. 2010; 98:301–308. [PubMed: 20065698]

Brouillet EP, Shinobu L, McGarvey U, Hochberg F, Beal MF. Manganese injection into the rat striatum produces excitotoxic lesions by impairing energy metabolism. Exp Neurol. 1993; 120:89–94. [PubMed: 8477830]

Crossgrove JS, Allen DD, Bukaveckas BL, Rhineheimer SS, Yokel RA. Manganese distribution across the blood-brain barrier: I. Evidence for carrier-mediated influx of managanese citrate as well as manganese and manganese transferrin. Neurotoxicology. 2003; 24:3–13. [PubMed: 12564377]

Crossgrove JS, Yokel RA. Manganese distribution across the blood-brain barrier: III. The divalent metal transporter-1 is not the major mechanism mediating brain manganese uptake. Neurotoxicology. 2004; 25:451–460. [PubMed: 15019308]

Finkelstein Y, Milatovic D, Aschner M. Modulation of cholinergic systems by manganese. Neurotoxicology. 2007; 28:1003–1014. [PubMed: 17920128]

Fujishiro H, Yano Y, Takada Y, Tanihara M, Himeno S. Roles of ZIP8, ZIP14, and DMT1 in transport of cadmium and manganese in mouse kidney proximal tubule cells. Metallomics. 2012; 4:700–708. [PubMed: 22534978]

Galvani P, Fumagalli P, Santagostino A. Vulnerability of mitochondrial complex I in PC12 cells exposed to manganese. Eur J Pharmacol. 1995; 293:377–383. [PubMed: 8748691]

Gavin CE, Gunter KK, Gunter TE. Mn^{2+} sequestration by mitochondria and inhibition of oxidative phosphorylation. Toxicol Appl Pharmacol. 1992; 115:1–5. [PubMed: 1631887]

Girijashanker K, He L, Soleimani M, Reed JM, Li H, Liu Z, Wang B, Dalton TP, Nebert DW. Slc39a14 gene encodes ZIP14, a metal/bicarbonate symporter: similarities to the ZIP8 transporter. Mol Pharmacol. 2008; 73:1413–1423. [PubMed: 18270315]

Gunter KK, Aschner M, Miller LM, Eliseev R, Salter J, Anderson K, Gunter TE. Determining the oxidation states of manganese in NT2 cells and cultured astrocytes. Neurobiol Aging. 2006a; 27:1816–1826. [PubMed: 16290323]

Gunter KK, Aschner MA, Miller LM, Eliseev R, Salter J, Anderson K, Hammond S, Gunter TE. Determining the oxidation states of manganese in PC12 and nerve growth factor-induced PC12 cells. Free Radic Biol Med. 2005; 39:164–181. [PubMed: 15964508]

Gunter TE, Gavin CE, Aschner M, Gunter KK. Speciation of manganese in cells and mitochondria: A search for the proximal cause of manganese neurotoxicity. Neurotoxicology. 2006b; 27:765–776. [PubMed: 16765446]

Gunter TE, Miller LM, Gavin CE, Eliseev R, Salter J, Buntinas L, Alexandrov A, Hammond S, Gunter KK. Determination of the oxidation states of manganese in brain, liver, and heart mitochondria. J Neurochem. 2004; 88:266–280. [PubMed: 14690515]

He L, Girijashanker K, Dalton TP, Reed J, Li H, Soleimani M, Nebert DW. ZIP8, member of the solute-carrier-39 (SLC39) metal-transporter family: characterization of transporter properties. Molecular Pharmacology. 2006; 70:171–180. [PubMed: 16638970]

Hentze MW, Muckenthaler MU, Andrews NC. Balancing acts: molecular control of mammalian iron metabolism. Cell. 2004; 117:285–297. [PubMed: 15109490]

Ivanov AI. Pharmacological inhibition of endocytic pathways: Is it specific enough to be useful? Methods in Molecular Biology. 2008; 440:15–33. [PubMed: 18369934]

Latimer, WM.; Hildebrand, JH. Reference Book of Inorganic Chemistry. The McMillan Company; New York: 1956.

Liu Z, Li H, Soleimani M, Girijashanker K, Reed JM, He L, Dalton TP, Nebert DW. Cd^{2+} versus Zn^{2+} uptake by the ZIP8 HCO_3-dependent symporter: kinetics, electrogenicity and trafficking. Biochemical & Biophysical Research Communications. 2008; 365:814–820. [PubMed: 18037372]

Malecki EA. Manganese toxicity is associated with mitochondrial dysfunction and DNA fragmentation in rat primary striatal neurons. Brain Res Bull. 2001; 55:225–228. [PubMed: 11470319]

Malthankar GV, White BK, Bhushan A, Daniels CK, Rodnick KJ, Lai JC. Differential lowering by manganese treatment of activities of glycolytic and tricarboxylic acid (TCA) cycle enzymes investigated in neuroblastoma and astrocytoma cells is associated with manganese-induced cell death. Neurochem Res. 2004; 29:709–717. [PubMed: 15098932]

Maynard LS, Cotzias GC. The partition of manganese among organs and intracellular organelles of the rat. J Biol Chem. 1955; 214:489–495. [PubMed: 14367406]

Ohgami RS, Campagna DR, Greer EL, Antiochos B, McDonald A, Chen J, Sharp JJ, Fujiwara Y, Barker JE, Fleming MD. Identification of a ferrireductase required for efficient transferrin-dependent iron uptake in erythroid cells. Nature Genet. 2005; 37:1264–1269. [PubMed: 16227996]

Ohgami RS, Campagna DR, McDonald A, Fleming MD. The Steap proteins are metalloreductases. Blood. 2006; 108:1388–1394. [PubMed: 16609065]

Richardson DS, Ponka P. The molecular mechanisms of the metabolism and transport of iron in normal and neoplastic cells. Biochim Biophys Acta. 1997; 1331:1–40. [PubMed: 9325434]

Roth JA, Feng L, Walowitz J, Browne RW. Manganese-induced rat pheochromocytoma (PC12) cell death is independent of caspase activation. J Neurosci Res. 2000; 61:162–171. [PubMed: 10878589]

Roth JA, Horbinski C, Higgins D, Lein P, Garrick MD. Mechanisms of manganese-induced rat pheochromocytoma (PC12) cell death and cell differentiation. Neurotoxicology. 2002; 23:147–157. [PubMed: 12224755]

Sheftel AD, Zhang A-S, Brown C, Shirihai OS, Ponka P. Direct interorganellar transfer of iron from endosome to mitochondrion. Blood. 2007; 110:125–132. [PubMed: 17376890]

Snedecor, GW.; Cochran, WG. Statistical Methods. Iowa State University Press; Ames, IA: 1989.

Trettel F, Rigamonti D, Hilditch-Maguire P, Wheeler VC, Sharp AH, Persichetti F, Cattaneo E, MacDonald ME. Dominant phenotypes produced by the HD mutation in STHdh(Q111) striatal cells. Human Mol Genet. 2000; 9:2799–2809. [PubMed: 11092756]

Vincent JB, Love S. The binding and transport of alternative metals by transferrin. Biochim Biophys Acta. 2012; 1820:362–378. [PubMed: 21782896]

West, RC., editor. CRC Handbook of Chemistry and Physics. the Chemical Rubber Co.; Cleveland, OH: 1971.

Yokel RA, Crossgrove JS. Manganese toxicokinetics at the blood-brain barrier. Research Report - Health Effects Institute. 2004; 119:7–73. [PubMed: 15043400]

Zwingmann C, Leibfritz D, Hazell AS. Energy metabolism in astrocytes and neurons treated with manganese: Relation among cell-specific energy failure, glucose metabolism, and intercellular trafficking using multinuclear NMR-spectroscopic analysis. J Cereb Blood Flow Metab. 2003; 23:756–771. [PubMed: 12796724]

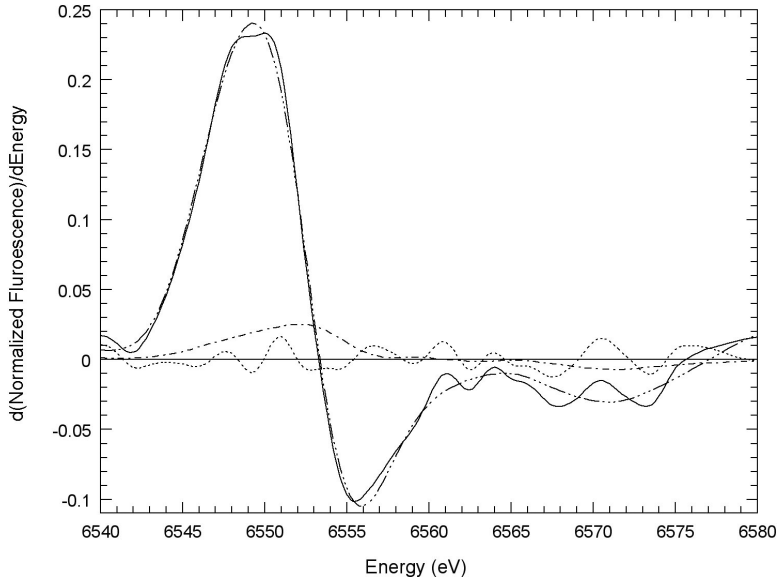

Fig. 1. XANES study of Mn^{3+}Tf formation

Best fit of first derivative model compound XANES spectra to the first derivative of the edge normalized XANES spectrum of Mn^{2+} incubated with apotransferrin. The sample was made up by mixing 2 mM Tf and 0.2 mM $MnCl_2$ in HEPES (10 mM, pH 7.2) buffered NaCl (160 mM) and incubated for 24 hours at 22° C. Also shown are the residual (Mn transferrin spectrum - best fit spectrum) and the spectrum of 0.17 times the edge-normalized first derivative spectrum of Mn^{3+} porphine for comparison. Mn transferrin (_____); best fit (__ .. __); residual (.....); 0.17 times d(Mn^{3+} porphine)/dE (_ _ _ _). The best fit is the sum of the first derivatives of the edge-normalized XANES spectra of 0.65 Mn^{2+} EGTA, 0.168 Mn^{2+} ATP, and 0.182 Mn^{3+} porphine. The R^2 of the fit is 0.996.

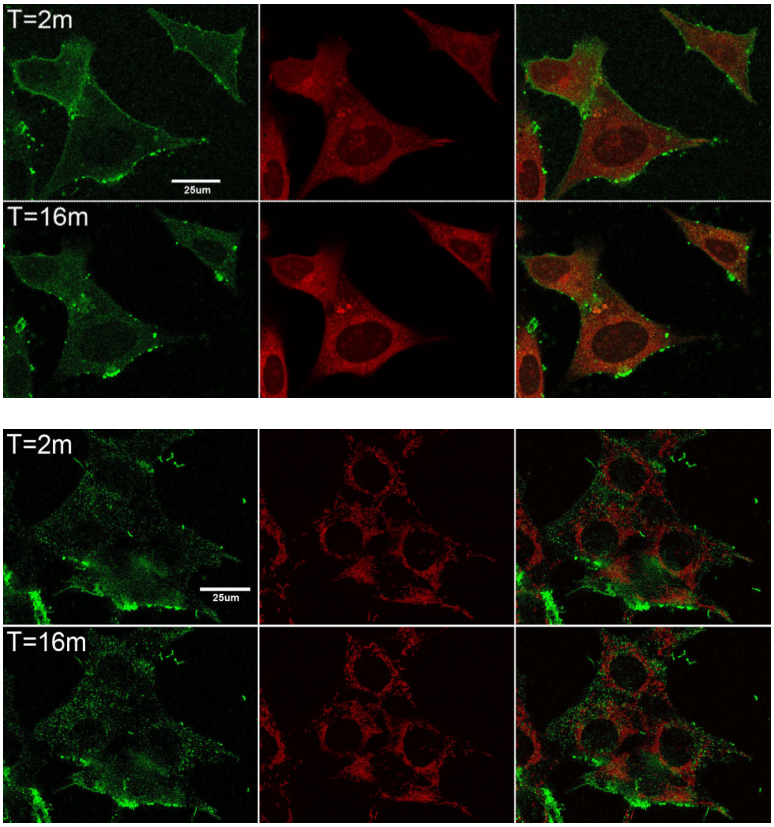

Fig. 2. Following AGMn^{3+}Tf uptake into cells using confocal microscopy

Confocal microscope images showing AGMn^{3+}Tf and mitotracker red in **A.** HT22 (hippocampal neurons) and **B.** STHdhQ7/Q7 (striatal neurons). The images in each set from left to right are AGMn^{3+}Tf (green) emission, mitotracker red (red) emission, and merged images. The top row in each set was taken 2 min after addition of 0.2 μM AGMn^{3+}Tf while the bottom row was taken 16 min after addition of the AGMn^{3+}Tf. Flow of medium through the cell holder was begun 1 min after addition of the AGMn^{3+}Tf in order to remove unbound fluorescent probe from the system. Initially the AGMn^{3+}Tf is found on the outside of the cell membranes but with time moves into the cell cytoplasm toward the mitochondrial network. The thickness of the Z planes in these images is between 0.15 and 0.3 μm.

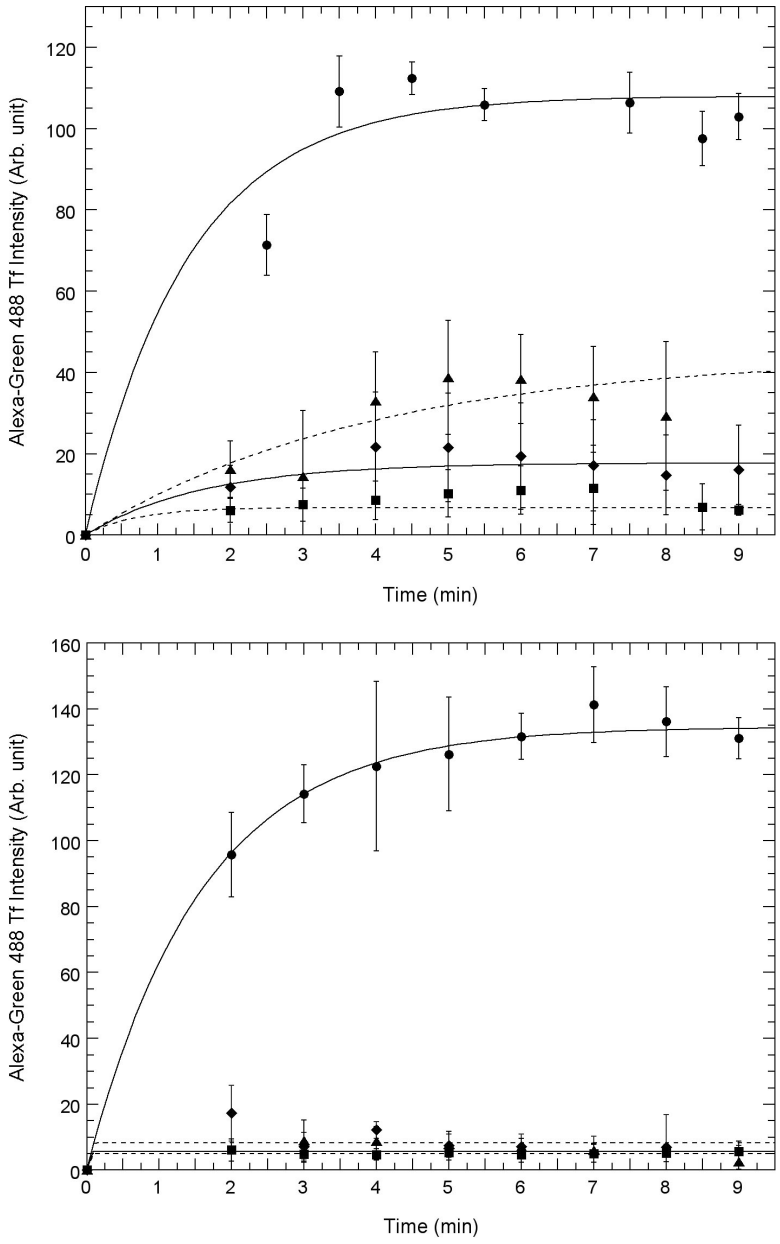

Fig. 3. Competition between uptake of $AGMn^{3+}Tf$ and $Fe^{3+}Tf$ and inhibition of uptake by chlorpromazine and dynasore using confocal microscopy

Uptake of $AGMn^{3+}Tf$ into the cell interior as measured by green emission ocurring within regions of interest drawn just inside the plasma membrane of **A.** HT22 (hippocampal) neurons and **B.** STHdhQ7/Q7 (striatal) neurons measured using "Image J" software obtained from NIH. 0.2 μM $AGMn^{3+}Tf$ was added at time zero in each of these experiments and excess $AGMn^{3+}Tf$ washed away with a flow of fresh medium at time 1 min with the flow of medium continuing for 1 min. Movement of the $AGMn^{3+}Tf$ into the neurons was determined by measuring the average emission intensity per unit area using Image J software inside the regions of interest drawn around the inside of the cell membrane as shown in supplementary figure S5. In these experiments, the regions of interest were drawn around the inside of the plasma membrane of each cell within the field of view and the average emission intensity per unit area taken and averaged over all of the cells. Control: 0.2

μM Mn^{3+}Tf no other additions (●): 80 μM Fe^{3+}Tf (■) was added and washed away before time zero; 30 μM chlorpromazine (◆) was added 10 min prior to time zero; 80 μM dynasore (▲) was added 10 min prior to zero time. The error bars represent ± 1 standard deviation of three independent measurements. The curves through the data points represent fits to the equation $y = m_1 + m_2(1\text{-}e^{-m3x})$ with each point weighted by its reliability and the values of m_1, m_2, and m_3 determined by the fit.

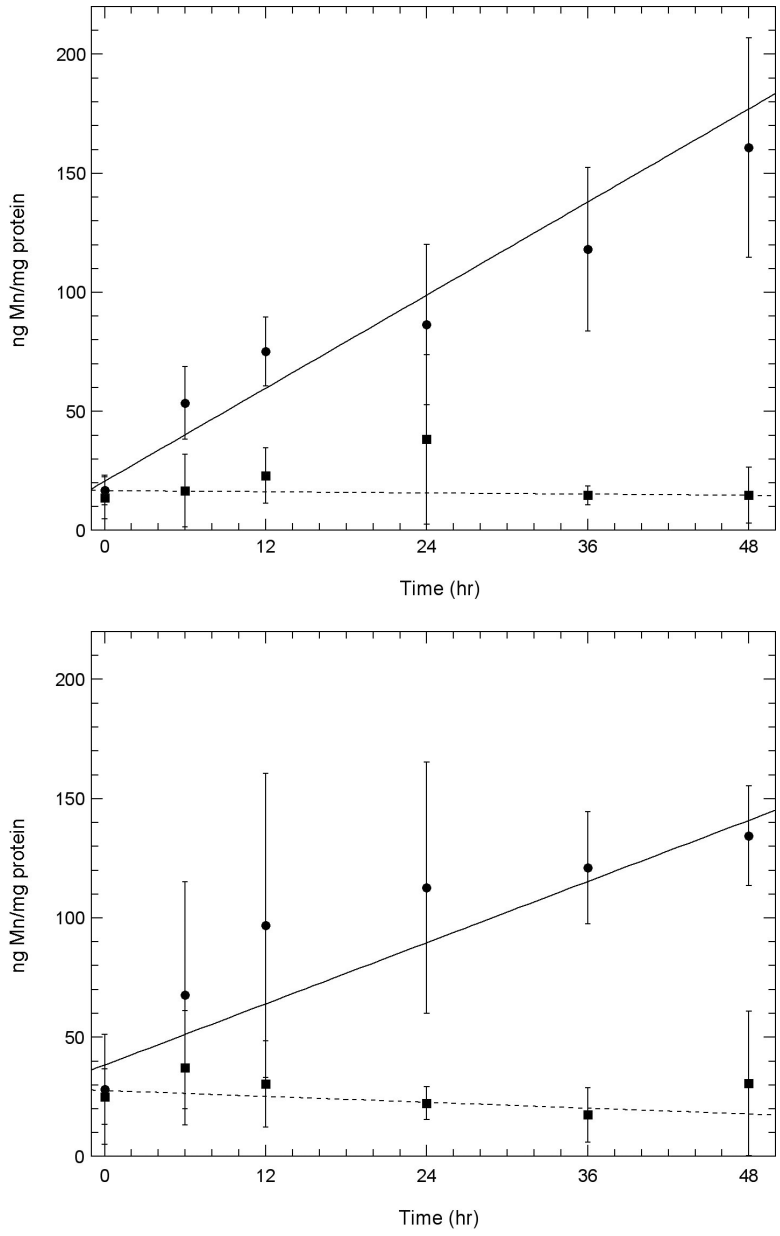

Fig. 4. A comparison of the amount of Mn uptake of Mn^{3+}Tf with that of the amount of Mn^{2+}impurity measured in the Mn^{3+}Tf sample in two neuronal cell lines

A. Uptake of Mn into HT22 (hippocampal) neurons and **B.** STHdhQ7/Q7 (striatal) neurons using atomic absorption. Experiments showing this Mn uptake were carried out as described under "Uptake of Mn^{3+}Tf by Neuronal Cells" in the Methods section. Uptake of Mn from 100 μM purified Mn^{3+}Tf (○) is compared with Mn uptake from 0.02 μM Mn^{2+} (chloride) (□). 0.2 μM Mn^{2+} was the concentration of impurity Mn^{2+} estimated to be present in the Mn^{3+}Tf stock from the EPR measurements. This was diluted by a further factor of ten in the low concentration Mn^{2+} experiment similar to the dilution of the Mn^{3+}Tf stock when 100 μM of the purified Mn^{3+}Tf was added to the neurons. The data represent averages of three AA measurements each from 2 independent experiments. Error bars represent ± 1 standard deviation. The lines fit to the data were determined by weighting each point by its reliability. Results of Willcoxon Mann-Whitney tests carried out on the 24, 36, and 48 hour points

indicate that for both the HT22 data and the STHdhQ7/Q7 data, the probability that the 100 μM Mn^{3+}Tf data is a separate population from the 0.2 μM Mn^{2+} data is approximately 99.9%. In other words uptake from impurity Mn^{2+} in the Mn^{3+}Tf sample cannot explain the uptake observed from the Mn^{3+}Tf sample.

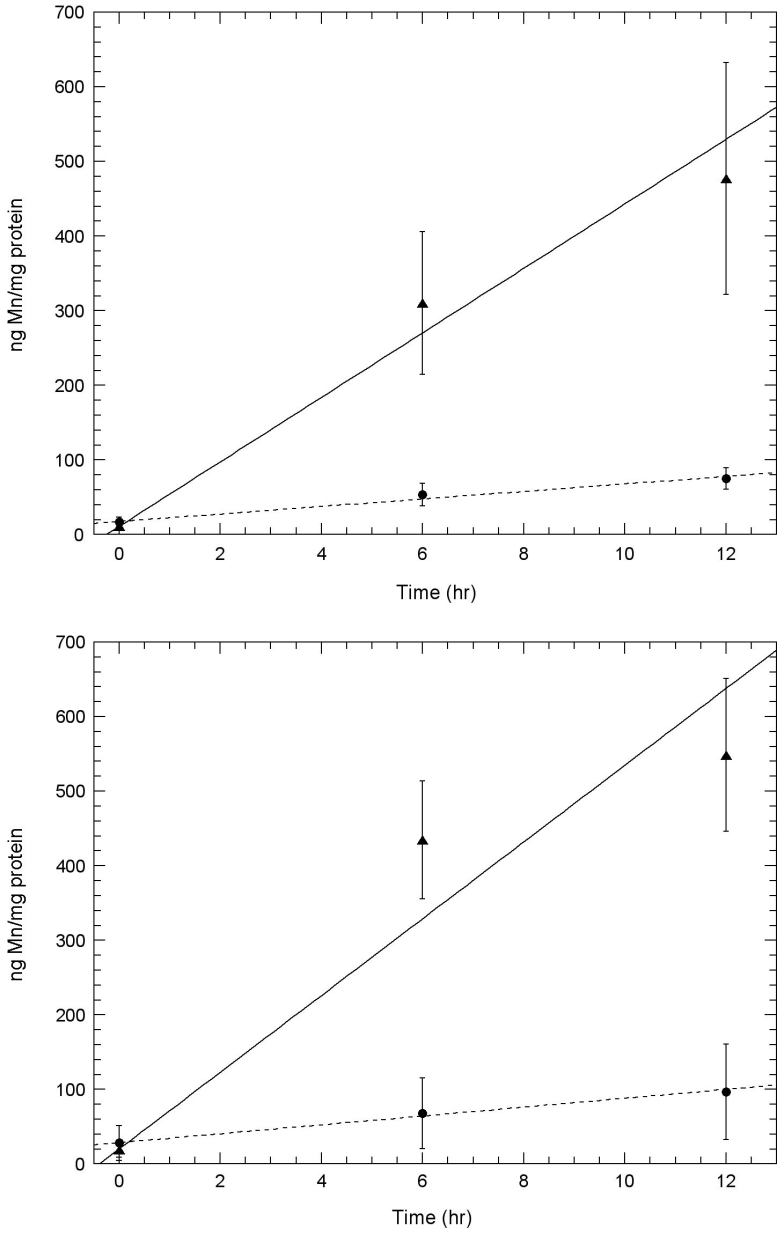

Fig. 5. A comparison of the amount of Mn uptake of Mn^{3+}Tf with that of the same molar amount of Mn^{2+} in two neuronal cell lines

A. Initial uptake measurements of Mn into HT22 (hippocampal) neurons and **B.** STHdhQ7/Q7 (striatal) neurons using atomic absorption comparing uptake from solutions containing 100 μM Mn^{3+}Tf (○) with that from 100 μM Mn^{2+} (chloride) (△). Experiments were carried out as described under "Uptake of Mn^{3+}Tf by Neuronal Cells" in the Methods section. The data represent averages of three AA measurements each from 2 independent experiments. Error bars represent ± 1 standard deviation. The lines fit to the data were determined by weighting each point by its reliability. Results of Willcoxon Mann-Whitney tests carried out on the 6 and 12 hour points indicate that for both the HT22 data and the STHdhQ7/Q7 data, the probability that the 100 μM Mn^{3+}Tf data is a separate population from the 100 μM Mn^{2+} data is greater than 99.4%. This indicates that uptake of 100 μM Mn^{2+} is significantly greater than uptake from 100 μM Mn^{3+}Tf in both these neuronal samples.